

Rare earth oxide films: their preparation and characterization

TADEUSZ WIKTORCZYK

Institute of Physics, Wrocław University of Technology, 50-370 Wrocław, Wybrzeże Wyspiańskiego 27, Poland.

The paper summarises the results of our investigations dealing with preparation of rare earth oxide films and examinations of their physical properties. Different deposition methods have been applied for fabrication of these films and rare-earth-oxide-based thin film coatings. Main results concerning film microstructure and optical properties in the wavelength range from the UV up to the IR are presented. Electrical and dielectric studies have been carried out in the time domain and in the frequency domain (from very low frequencies up to radio frequencies) for selected rare earth oxides. MIM sandwich-type structures have been fabricated for this aim. Trapping levels in these oxides have been investigated. The complex impedance diagnostics was applied to analysis of the volume of R_2O_3 film and interfacial properties (metal/insulator barriers) of $M/R_2O_3/M$ thin film structures.

1. Introduction

Rare earth elements and different rare earth compounds have been in the focus of interest of scientists and researchers for the last 50 years. Rare earth oxides (REO) are an important group, which can be distinguished from among many rare earth compounds. This group consists of the oxides of 17 elements in the periodic system, *i.e.*, lanthanum, the lanthanide, scandium and yttrium, which have been intensively investigated. The REO have been the subject of a large number of publications. Many review papers published in scientific journals and books which appeared to date have been devoted to preparation of the REO, their structure, physicochemical properties and also possible applications [1]–[8].

Since the 60's a great progress in thin-film technology has been observed [9]–[13]. Many different materials have been prepared in a thin-film form. Thin films have been fabricated as simple planar coatings on dielectrics, semiconductors and metals or in a sandwich type structures (*i.e.*, MIM, MOS, MOM, MOSFET, *etc.*, structures). These works have been performed mainly as a result of examinations of the basic physical and material properties of thin films as well as due to their potential application. First works devoted to preparation of the REO films, their optical, dielectric and electrical properties were published at the end of 50's [14]–[18].

We started examination of the REO thin films in the 70's. Our first papers were devoted to elaboration of reproducible fabrication methods for the REO thin films and to examination of their basic physical properties. Then our interest was focused on optical, dielectric and electrical properties of the REO thin film coatings and REO thin film structures. Results of these investigations have been published in scientific journals, conference proceedings and reports [19]–[63]. Optical and electrical properties of the REO thin films were also the subject of Ph.D. theses [64]–[66].

The aim of this paper is to present and summarise results of the investigation carried out by our Thin Film Group, dealing with preparation and characterization of the REO thin films, which covers the period up to the year 2000.

2. Preparation of rare earth oxide thin films

In the bulk state all the REO form sesquioxides, R_2O_3 ($R \equiv La, Ce, \dots, Y$ and Sc). Some of the REO form dioxides, RO_2 ($R \equiv Ce, Pr$ and Tb). For Ce, Pr and Tb the intermediate oxides, RO_x (where $1.5 < x < 2$) are also known [1]. According to [4] the monoxides, RO , can be formed in the gas state only at high temperatures in a vacuum. In solid state only EuO is well-established [4]. The monoxides of some other rare earth metals can be observed in the bulk state at high temperatures under high pressure. The REO have been known as the high temperature oxides which melt in the temperature range from 2300 to 2500 °C [1], [3], [6].

Different preparation methods have been applied to fabrication of the REO thin films and to REO-based thin-film coatings. These methods include both physical as well as chemical deposition. Some of these techniques have been applied to preparation of the REO films in our laboratory. In fabricating thin films we used the following methods:

a) Thin films were produced by thermal evaporation of the REO from resistance heaters. Tungsten boats were used as evaporation source. These depositions were carried out in the vacuum chamber under the oxygen partial pressure of 8×10^{-5} Tr (1×10^{-2} Pa).

b) Thin films were prepared by the reactive evaporation of the rare earth metal in oxygen, at a pressure of 4×10^{-4} Tr (5×10^{-2} Pa).

c) The REO thin films were fabricated by the method of electron-beam depositions in a vacuum.

d) Thin films were obtained by thermal oxidation of the rare earth metal films previously deposited onto respective substrates.

Many papers can be found in the literature which deal with the physical properties of thin films prepared by direct evaporation of the REO from resistance sources (mainly from tungsten heaters) [67]–[88]. These investigations were performed due to potential application in thin-film optics and microelectronics. However, poor reproducibility of the physical parameters for films prepared with such a technology was reported by some investigators [14], [36], [87].

We have shown [25], [26] that films deposited by direct evaporation from tungsten sources contain tungsten impurities. These impurities exist in the form of tungsten oxides. The content of the non-stoichiometric tungsten oxide depends on the temperature of a resistance heater and the type of rare earth metal. The X-ray microanalysis of the films have shown that tungsten contamination of such films may reach a level from about 5 weight percent for Gd_2O_3 up to about 18 weight percent for Yb_2O_3 [25], [26]. At present, a simple evaporation from resistance heater seems to be a poor preparation method of the REO films.

A satisfactory quality of thin film coatings and thin film structures has been obtained with the methods (b), (c) and (d). These methods have been reported in papers [89]–[104] to be also successfully applied to deposition of the REO films. However, it has been found that the best method of producing of the REO films is the evaporation of the rare earth metal oxide with the help of an electron gun. We have been applied quartz and glass plates as the evaporation substrates. Films for optical investigations have been deposited onto MgF_2 , KRS-5, KBr and Si substrates. The NaCl monocrystals have also been used as substrates for films evaporated for structural examinations purposes.

Al electrical, dielectric and photoconductivity studies as well as examinations of thermally stimulated currents were carried out on $M/R_2O_3/M$ thin film sandwich type structures [20], [34], [51]. These structures (thin-film capacitors) were deposited onto quartz or glass substrates with the use of specially arranged mechanical masks. The areas of thin film capacitors were in the range $0.1 - 10 \text{ mm}^2$.

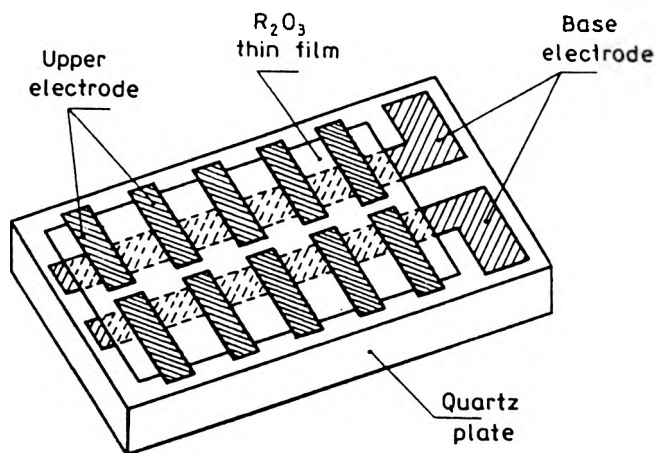


Fig. 1. Typical configuration of $M/R_2O_3/M$ thin film sandwiches fabricated for dielectric and electrical measurements.

However, most of the specimens under examination had the area of about $1 - 1.5 \text{ mm}^2$. Sample thickness (*i.e.*, thickness of the REO films) ranged from 0.020 to $2 \mu\text{m}$. A quartz-crystal monitor was applied for film thickness monitoring during film deposition. Finally optical interference methods were used for film thickness

measurements after deposition. Typical deposited structures consisted of 10 thin film capacitors deposited onto each plate (Fig. 1).

3. Film microstructure

It is known that under suitable conditions the rare earth sesquioxides form five types of the polymorphic structures designated as types A, B, C, H and X. However, for temperatures below about 2000 °C only hexagonal (A-type), monoclinic (B-type), and body centred (C-type) structures have been observed [1]–[3]. The structure of rare earth oxides in a thin film form has been investigated by many researchers. A review article summarizing structural examinations of the REO films was published by GASGNIER [4].

In order to identify the deposited material and its structure we applied X-ray electron diffraction methods as well as transmission electron microscope observations (TEM micrographs). Dron-1 type X-ray diffractometer and Philips EM-310 electron microscope were used for this aim. Structural examinations were carried out for Eu_2O_3 [24], Gd_2O_3 [30], [64], Dy_2O_3 [48], Ho_2O_3 [61] and Yb_2O_3 [25], [36], [66] thin films.

We have shown that films obtained by thermal evaporation of R_2O_3 from tungsten boats are completely amorphous independent of the deposition parameters [36], [64]. Films obtained by thermal oxidation of polycrystalline metal films at a temperature of 423 K were also amorphous [36].

Thin films obtained by electron beam deposition or by reactive evaporation of the rare earth metal in oxygen were amorphous in nature or polycrystalline depending on conditions under which they were obtained. The main parameters which influence the ordering of the film structure are: elevated temperature of substrate and increased pressure during evaporation as well as thermal annealing after deposition.

Films deposited onto unheated substrates with the help of an electron gun or by reactive evaporation of the rare earth metal in the oxygen were amorphous or polycrystalline bordering on amorphous. Only one up to a few diffusive diffraction rings have been observed in diffraction patterns for such films. Films deposited at the oxygen pressure of $(2-8) \times 10^{-5}$ Tr ($3 \times 10^{-3} - 1 \times 10^{-2}$ Pa) onto heated substrates (up to $T = 473 - 535$ K) were polycrystalline with a grain size of about 10–14 nm. A well-marked texture was observed in X-ray diffraction patterns for Gd_2O_3 [30] and Yb_2O_3 [36] films deposited onto heated substrates or for films themally annealed at 673 K. The R_2O_3 films recrystallized easily, however, as a result of electron beam irradiation during TEM examinations. Such a recrystallization followed due to sharply focused electron beam that caused film heating. Large crystals (up to 0.2–2 μm in size) were observed in Dy_2O_3 [48], Ho_2O_3 [61] and Yb_2O_3 [36] films heated with an electron beam.

On the basis of the electron and X-ray diffraction patterns we could state that all diffraction rings we observed for the REO films correspond with the most intensive

rings for R_2O_3 powders (literature data) and are consistent with those of bulk-centred cubic structure for rare earth metal sesquioxide (*C*-type structure of R_2O_3).

4. Optical properties

Experimental examinations of the optical properties of thin films are based on two main groups of measuring techniques, namely: i) the spectrophotometric methods which rely on the measurements of specimen's transmittance T or reflectance R versus the wavelength, and ii) the polarization methods which deal with the measurements and analysis of light polarity for the light reflected of the specimen.

Both of these methods have been applied in our laboratory for optical examinations of the REO thin films since the 70's [21], [22], [24]–[33], [48], [62]. Most of the papers published up to 1974 were devoted to optical examinations of thin films fabricated by a simple vacuum deposition of the REO from commonly used sources (tungsten, molybdenum or tantalum boats). Films fabricated with such a technique exhibit strong absorption in the ultraviolet, showing also a considerable absorption in the violet [14], [25]. This absorption can be reduced by annealing the specimens for many hours. Films deposited by evaporation from resistance heaters have high refractive index $n = 1.8 - 2.2$ at 600 nm which in some cases is even higher than that for monocrystals [14], [25], [64]. We have shown that such a behaviour is connected with high impurity concentration coming from evaporation sources [25], [26]. For some of the REO these impurities were a risen of very non-reproducible optical properties of thin films [14], [25], [26]. Systematic optical investigations have been carried out for thin film oxides of praseodymium, europium, gadolinium, terbium, dysprosium, holmium, erbium, ytterbium and lutetium deposited with the help of an electron gun.

4.1. Spectral characteristics of transmittance and complex refractive index

The dielectric properties of any thin film for optical frequencies are described by the complex refractive index

$$n^*(f) = n(f) - jk(f). \quad (1)$$

The knowledge of spectral characteristics of the real part of the refractive index and the extinction coefficient is important not only from the physical point of view, but also due to possible applications of the given material in optical instruments and devices.

For thin dielectric and semiconductor films the $R(\lambda)$ and $T(\lambda)$ spectral characteristics enable observation of the interference effects. Optical transmittance of the parallel-plate uniform thin film characterized by the complex refractive index $n_1^* = n_1 - jk_1$ deposited onto non-absorbing substrate can be expressed by general equation [105]

$$T = \frac{8n_0n_2(n_1^2 + k_1^2)}{Ech\eta + Fsh\eta - G\cos\zeta + H\sin\zeta} \quad (2)$$

in which: $E = (n_1^2 + k_1^2 + n_0^2)(n_1^2 + k_1^2 + n_2^2) + 4n_1^2 n_0 n_2$,
 $F = 2n_1 [n_2(n_1^2 + k_1^2 + n_0^2) + n_0(n_2^2 + k_1^2 + n_1^2)]$,
 $G = (n_1^2 + k_1^2 - n_0^2)(n_1^2 + k_1^2 - n_2^2) - 4n_0 n_2 k_1^2$,
 $H = 2k_1 [n_2(n_1^2 + k_1^2 - n_0^2) + n_0(n_2^2 + k_1^2 - n_1^2)]$,
 $\eta = 4\pi k_1 d/\lambda$, $\zeta = 4\pi n_1 d/\lambda$, d – film thickness, n_2 – refractive index of the substrate,
 n_0 – the refractive index of the "first medium" (the air), λ – the wavelength.

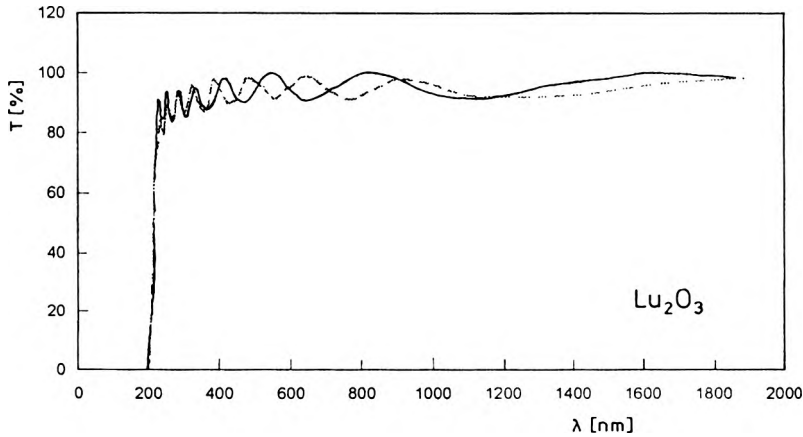


Fig. 2. Dependence of the transmission coefficient T upon the wavelength λ for Lu_2O_3 thin films deposited at different oxygen pressures: $p = 5 \times 10^{-6}$ Tr (7×10^{-4} Pa), $d = 457$ nm (solid line) and $p = 8 \times 10^{-5}$ Tr (1×10^{-2} Pa), $d = 513$ nm (broken line).

In Figure 1, $T(\lambda)$ characteristics for Lu_2O_3 thin films are presented [62]. Such transmittance characteristics are typical for all R_2O_3 films. The range of good transparency for R_2O_3 films starts from about 0.2–0.3 μm and lasts up to the near-infrared, depending on the REO, film thickness and on conditions during film fabrication. The interference effects are well seen in this region. As-deposited films of terbium and praseodymium exhibit high absorption in the UV and the visible-range and correspond with Tb_4O_7 and Pr_6O_{11} film stoichiometry, respectively. After reduction process in the hydrogen atmosphere these films transformed into sesquioxides [27], [28]. Such films had spectral characteristics of the transmittance similar to those of other sesquioxides. Exemplary transmittance characteristics for Pr_6O_{11} and Pr_2O_3 thin films obtained by MARCINÓW [28] are shown in Fig. 3.

The Gd_2O_3 thin films have been investigated in the infrared, in a wide wave spectrum range up to 50 μm [26], [30]. A typical dependence of transmittance on the wavelength is presented in Fig. 4. In the region investigated the Gd_2O_3 thin films – regardless of the evaporation technique and kind of the substrate – have absorption bands localised at 3, 7, 11.7 and 25 μm . They were described in the following way:

- the absorption band at 3 μm results from the O–H stretching mode,
- the double band at 7 μm and very weak absorption band at 11.7 μm (for films thicker than 0.7 μm) are due to the CO_3^- ions in the carbonate compounds,

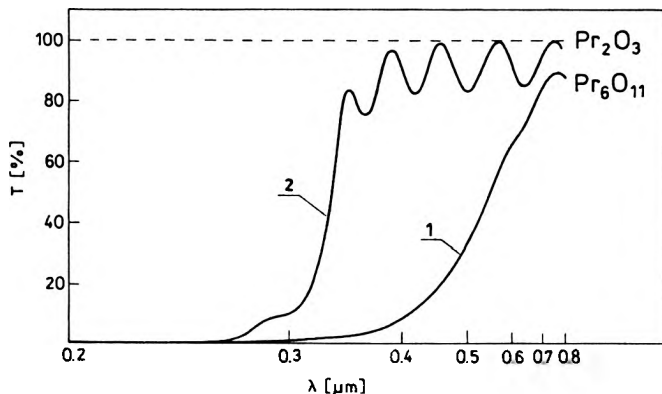


Fig. 3. Spectral dependence of the transmission coefficient for Pr_2O_3 and Pr_6O_{11} thin films of thickness 545 nm. Curve 1 is plotted for Pr_6O_{11} films. Curve 2 shows $T(\lambda)$ characteristic for films prepared by the reduction of Pr_6O_{11} films in the hydrogen furnace at 973 K. Film thickness – 545 nm.

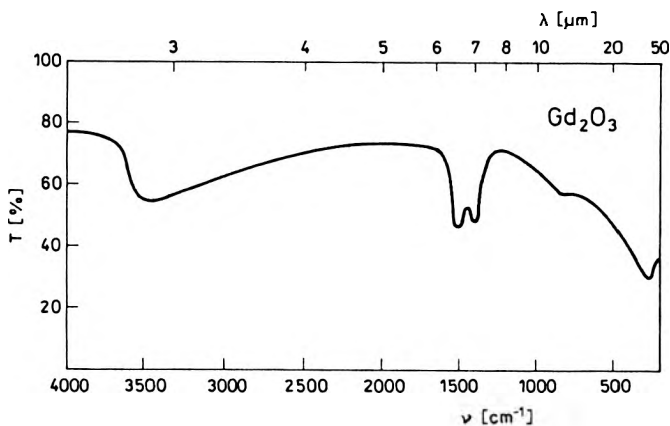


Fig. 4. Infrared transmittance of Gd_2O_3 film 1 μm thick, evaporated onto KRS-5 substrate.

c) the absorption band at 25 μm is connected with the centre of lattice vibration of Gd_2O_3 .

The absorption bands at 3, 7 and 11.7 μm resulted from residual gases incorporated into the films during evaporation process.

The refractive index of thin films can be evaluated from Eq. (2) by application of the numerical methods. A special evaluation method has been applied to this aim [106]. TRUSZKOWSKA, BOROWICZ and WESOŁOWSKA [32] have estimated optical constants of the REO films by the numerical fitting of the $T(\lambda)$ data. However, most literature which provides for estimation of the optical constants deals with different approximation of the general formula expressed by Eq. (2). In the simplest case, neglecting film absorption, this formula can be rewritten [11], [105].

$$T = \frac{8n_0 n_2 n_1^2}{(n_0^2 + n_1^2)(n_1^2 + n_2^2)^2 + 4n_0 n_1^2 n_2 + (n_1^2 - n_0^2)(n_2^2 - n_0^2) \cos \xi} \quad (3)$$

Assuming $n_0 < n_1 > n_2$, the transmittance reaches extreme values T_{\max} and T_{\min} for optical thicknesses of the film: $n_1 d = 1/2 m \lambda$, $n_1 d = 1/4(2m+1)\lambda$, respectively (m is the interference order). The refractive index can be easily evaluated for these extremes of the transmittance. The simplified methods given by HALL and FERGUSON [107], SCHULTZ and TANGHERLINI [108] and VRIENS and RIPPENS [109] have also been applied by us to evaluation of optical constants of the REO films.

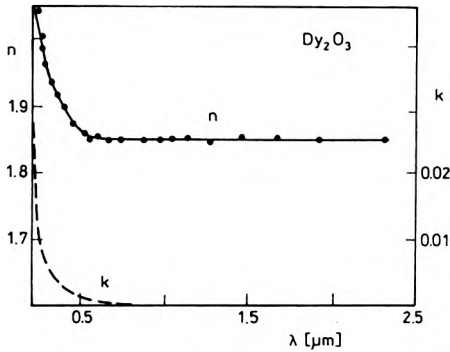


Fig. 5. Dependence of the refractive index n and extinction coefficient k for Dy_2O_3 films on the wavelength. Film thickness: $d = 526$

Table 1. The refractive index of rare earth oxide films.

Rare earth oxide	$n(\lambda = 0.55 \mu\text{m})$	$n(\lambda = 1 \mu\text{m})$	References
Pr_2O_3	2.05	2.01	[28]
Pr_6O_{11}	1.98	1.91	[28]
Eu_2O_3	1.86	1.84	[24], [26]
Gd_2O_3	1.92	1.91	[26], [30]
Tb_2O_3	1.88	1.83	[27]
Tb_4O_7	2.29	1.87	[27]
Dy_2O_3	1.86	1.85	[48]
Ho_2O_3	1.80	1.79	[61]
Er_2O_3	1.88	1.87	[26]
Yb_2O_3	1.91	1.90	[21], [25], [26]
Lu_2O_3	1.84	1.83	[62]

Typical dispersion characteristics of the optical constants $n(\lambda)$ and $k(\lambda)$ for Dy_2O_3 films are shown in Fig. 5. The refractive index of all the films under examination has a small dispersion in the wavelength range $0.5 - 2.5 \mu\text{m}$. The R_2O_3 films exhibited very small absorption for a visible and infrared range. Values of the extinction coefficient for most REO films were below 0.01 for $\lambda > 350 \text{ nm}$. Values of the refractive index estimated by us for different rare earth oxides at $\lambda = 0.55 \mu\text{m}$ and $\lambda = 1 \mu\text{m}$ are

compiled in Table 1. Except for Pr_2O_3 films, values of the refractive indexes for rare earth sesquioxide layers at $\lambda = 0.55 \mu\text{m}$ are in the deficient range $1.8 - 1.92 \mu\text{m}$.

4.2. Optical application of the REO films: anti-reflection coatings

Optical examinations of thin films are important due to their potential application in optical instruments. The REO layers on quartz and glass exhibit very good adhesion. The REO coatings show high resistance to laser-beam irradiation in the near-infrared (at $\lambda = 1.06 \mu\text{m}$) [29]. These properties classify them as useful in applications. We have proposed to apply the REO films to antireflection coatings. A single, a double and a triple layer coating are commonly used. Two types of such coatings were fabricated by us on the basis of the REO films:

- a single layer coating of S-L($\lambda/4$) type on semiconductor substrates,
- a double layer coating of a S-H($\lambda/4$)L($\lambda/4$) type on glass substrates (S denotes here the substrate, H and L are the high and low refractive index materials, respectively).

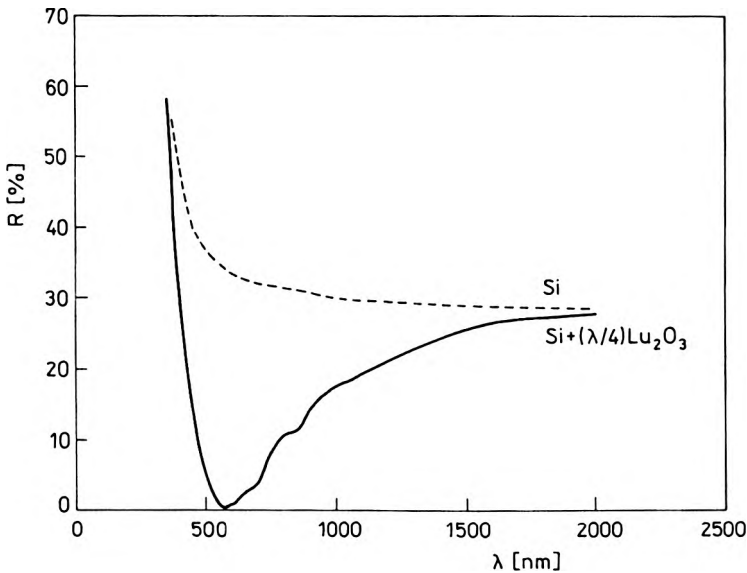


Fig. 6. Spectral dependence of the reflectance for a single layer $\text{Lu}_2\text{O}_3(\lambda/4)$ anti-reflection coating on silicon substrate. The broken line shows the reflectance of the pure silicon wafer.

Spectral characteristic of the reflection coefficient of the first type of coating is shown in Fig. 6 [62]. This is a $\text{Lu}_2\text{O}_3(\lambda/4)$ anti-reflection coating on silicon wafers. The $\text{Yb}_2\text{O}_3(\lambda/4)\text{MgF}_2(\lambda/4)$ and $\text{Gd}_2\text{O}_3(\lambda/4)\text{MgF}_2(\lambda/4)$ anti-reflection coatings of the second type were fabricated on glass substrates [29]. Spectral characteristic of the reflection coefficient for $\text{Gd}_2\text{O}_3(\lambda/4)\text{MgF}_2(\lambda/4)$ anti-reflection coating on a glass substrate is shown in Fig. 7. The results show that it is easy to produce very useful REO-based anti-reflection coatings with minimum reflectance below 1%.

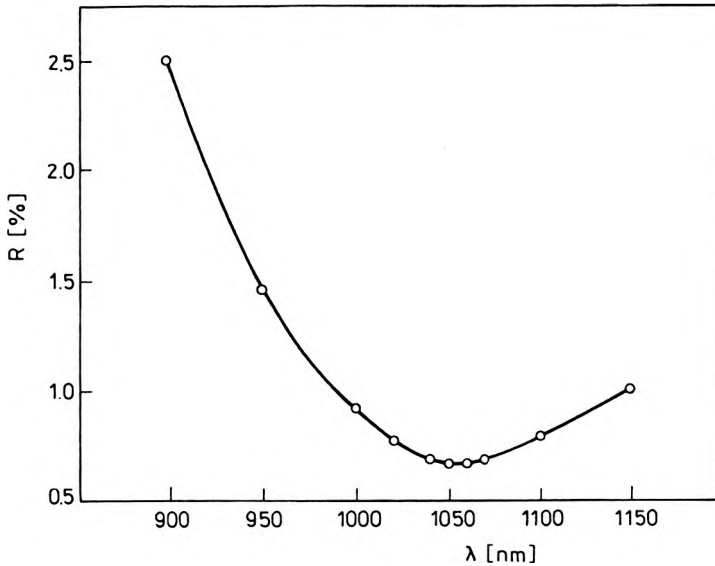


Fig. 7. Spectral dependence of the reflectance for a double layer $\text{Gd}_2\text{O}_3(\lambda/4)\text{MgF}_2(\lambda/4)$ anti-reflection coating on BK-7 glass substrate.

5. Electrical properties of $\text{M}/\text{R}_2\text{O}_3/\text{M}$ thin films structures

Electrical conductivity of the REO for baked powder samples has been examined by different researchers for high temperature range, *i.e.*, for $573 \text{ K} < T < 1846 \text{ K}$ [110]–[113]. These examinations show that both electrons and ions take part in electrical conductivity in R_2O_3 . Most of the rare earth sesquioxides exhibit very good insulating properties.

We started examinations of the electrical properties of some REO in a thin film form at the end of the 70's. Vacuum deposited $\text{M}/\text{R}_2\text{O}_3/\text{M}$ ($\text{M} \equiv \text{Dy}, \text{Ho}, \text{Yb}$) thin film sandwich-type structures were examined. The first works on that subject dealt with development of measuring techniques and with fabrication of MIM structures, as well as influence of preparation methods on electrical properties of rare earth oxides [23], [35], [36], [66]. Electrical properties of $\text{M}/\text{R}_2\text{O}_3/\text{M}$ structures were repeatable and stable in time, except for the films prepared by vacuum deposition of the REO from resistance heaters.

5.1. Electrical conductivity

Different techniques were applied for determination of the electrical conductivity of $\text{M}/\text{R}_2\text{O}_3/\text{M}$ structures:

a) The conductivity was estimated from measurements of charging currents. The "equilibrium current" I_{dc} was reached after the time of $10^2 - 10^5 \text{ s}$ [36].

b) The conductivity was determined with the method of slow cooling of specimens at applied voltage [53].

c) The conductivity was evaluated from relation (4) by measuring the charging $I_c(t)$ and discharging current $I_d(t)$ after the time t [41]

$$I_{dc} = I_c(t) - I_d(t). \quad (4)$$

At room temperature the low field d.c. resistivity of $M/\text{Dy}_2\text{O}_3/M$, $M/\text{Ho}_2\text{O}_3/M$ and $M/\text{Yb}_2\text{O}_3/M$ thin film sandwiches was very high, $\rho = 10^{11} - 10^{14} \Omega\text{m}$, which is comparable with resistivity of the other high-resistivity MIM thin film structures [36], [41]. Temperature dependence of the d.c. conductivity for $M/\text{R}_2\text{O}_3/M$ structures was measured. Typical temperature characteristics of d.c. conductivity current for $\text{Al}/\text{Dy}_2\text{O}_3/\text{Al}$ structures in $\log I \propto T^{-1}$ scale measured at different voltages are shown in Fig. 8 [53]. We can conclude from these measurements that electrical conductivity of $M/\text{R}_2\text{O}_3/M$ structures can be described by typical Arrhenius type formula

$$\sigma = \sigma_{01} e^{-E_1/kT} + \sigma_{02} e^{-E_2/kT} + \sigma_{03} e^{-E_3/kT}, \quad (5)$$

in which k is Boltzmann constant and T is a temperature. E_1 , E_2 and E_3 are respective activation energies for conduction process and σ_{01} , σ_{02} and σ_{03} are preexponential factors. The first term in Eq. (5) is responsible for the conductivity in the temperature range $400 \text{ K} < T < 500 \text{ K}$, the second one decides on the conductivity at temperatures $300 \text{ K} < T < 400 \text{ K}$, while the last one describes the conductivity

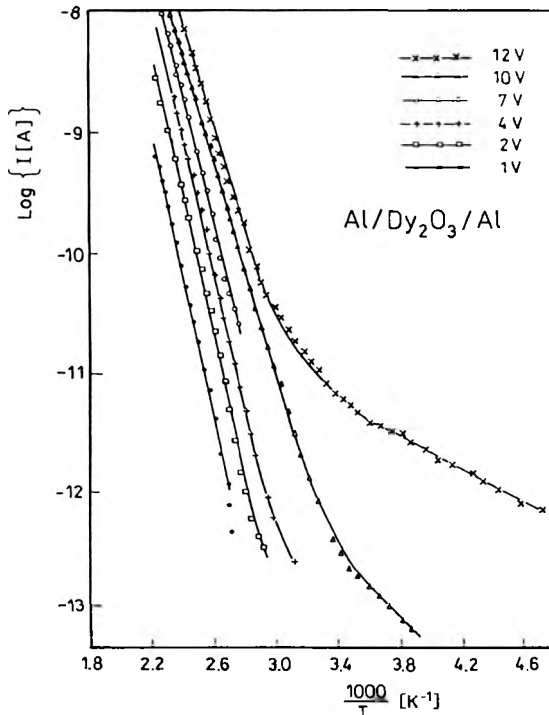


Fig. 8. Temperature dependence of the conductivity current for $\text{Al}/\text{Dy}_2\text{O}_3/\text{Al}$ thin film sandwiches measured at different voltages in $\log I \sim 1000/T$ scale. Dy_2O_3 film thickness $d = 146 \text{ nm}$.

at low temperatures. Values of the high-temperature activation energy E_1 for the samples examined were in the range 0.9–1.23 eV [35], [36], [41], [43], [51], [58]. The experimental data show that the activation energy E_1 depends on applied voltage and is connected with deep Coulombic centres. The activation energy E_2 reached values of 0.54 eV for M/Yb₂O₃/M structures [36] and 0.32 eV/0.55 eV for M/Dy₂O₃/M structures [47]. At low temperatures, *i.e.*, for 100 K < T < 200 K, the conductivity was almost temperature independent. Values of the activation energy E_3 were in the range 0.01–0.03 eV (for M/Dy₂O₃/M thin-film structures). The hopping type conductivity was involved for the explanation of the low-temperature d.c. electrical conductivity in these structures [53].

5.2. Current-voltage characteristics

The current voltage ($I-V$) characteristics for M/R₂O₃/M thin film structures measured for temperatures between 200 K and 500 K have been presented in the papers [23], [35], [58], [60]. For all the specimens examined low-voltage $I-V$ characteristics were linear (*i.e.*, Ohmic): $I \propto V^1$. For high electrical fields (*i.e.*, for $F \geq 10^5$ V/cm), the $I-V$ characteristics exhibited non-linear behaviour: $I \propto V^n$. Values of the exponent n were in the range between 1 and 12 [36], [60] and depended on the temperature, applied voltage, material of capacitor electrodes and on film preparation method.

To explain the $I-V$ characteristics different conductivity mechanisms including bulk effects as well as processes responsible for carrier transport across M/I contacts have been taken into account [23], [24], [66]. Experimental investigations of M/Yb₂O₃/M structures show that usually barrier-type contacts are formed at M/Yb₂O₃ interfaces. Ohmic electrodes are formed only at Yb/Yb₂O₃ contacts obtained by thermal oxidation of Yb films [63].

5.3. Isothermal non-steady state currents

The method of isothermal non-steady state currents or dielectric-relaxation-currents (IDRC) was applied to electrical examinations of M/R₂O₃/M thin film capacitors [41], [43], [52], [60], [63]. The method consists of the time domain measurements of the charging $I_c(t)$ and discharging currents $I_d(t)$. The $I_c(t)$ currents were measured after application of a step voltage U to the sample at a time $t = 0$. The $I_d(t)$ currents were measured after voltage removing.

Typical families of the isothermal charging and discharging currents for Al/Ho₂O₃/Al-type capacitors are shown in Figs. 9 and 10, respectively [52]. The discharging currents follow the relations:

$$I_c(t) \propto t^{-n} \quad \text{for short times,} \quad (6)$$

$$I_d(t) \propto t^{-m} \quad \text{for long times,} \quad (7)$$

which express the "universal dielectric response law" [114], [115].

For short times the charging currents have the same character as the discharging currents. For long times the charging currents reach a constant value and correspond

to the conductivity current (I_{dc}) at a given temperature. Values of the parameter n were in the range 0.22–0.60 for Al/Dy₂O₃/Al [41], [45] about 0.4 for Al/Ho₂O₃/Al [52] and 0.38–0.5 for Al/Yb₂O₃/Al [43], [60]. Values of the exponent m changed

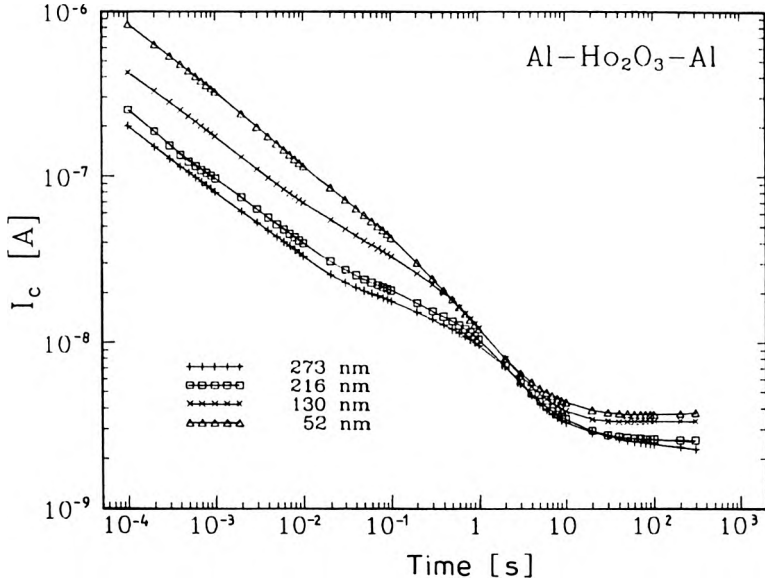


Fig. 9. Time dependence of the charging current $I_c(t)$ for Al/Ho₂O₃/Al structures with different insulator thicknesses measured at a temperature of 473 K.

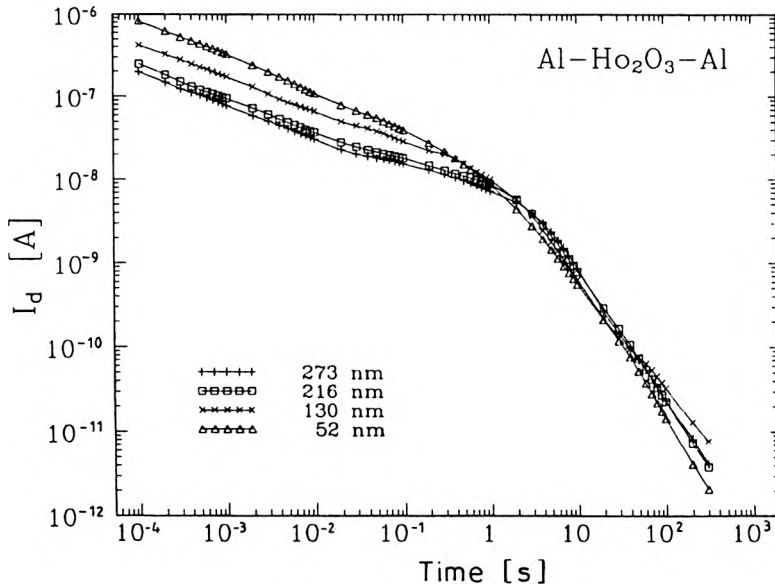


Fig. 10. Time dependence of the discharging current $I_d(t)$ for Al/Ho₂O₃/Al structures with different insulator thicknesses measured at a temperature of 473 K.

between 0.9 and 1.5. The $I_d(t)$ characteristics in this range depend on the metal applied as capacitor electrodes [60]. Such a behaviour shows an important role of electrodes in long-time dielectric relaxation characteristics. In paper [63], the charge released during relaxation process was estimated. These results were explained under assumption of the response of two Schottky barriers at M/I electrodes.

6. Dielectric properties

The dielectric properties of any insulating film can be characterized by the complex capacitance, usually determined from measurements

$$C^*(\omega) = C'(\omega) - jC''(\omega) = C(\omega) - \frac{jG(\omega)}{\omega}, \quad (8)$$

C' and C'' denote the real and imaginary parts of the capacitance, respectively. $C(\omega)$ and $G(\omega)$ are the parallel electric capacitance and the total conductance of the specimen, at a circular frequency ω ($\omega = 2\pi f$).

The complex dielectric permittivity $\varepsilon^*(\omega)$ is related to C^* by a geometrical factor $C_0 = \varepsilon_0 s/d$

$$\varepsilon^*(\omega) = \frac{C^*(\omega)}{C_0} = \varepsilon'(\omega) - j\varepsilon''(\omega) \quad (9)$$

where ε_0 is the dielectric permittivity of a free space, s is sample area and d – its thickness.

Very often in technical applications the dielectric loss factor, $\tan \delta$ is also used for material characterization

$$\tan \delta = \frac{G(\omega)}{\omega C(\omega)} = \frac{\varepsilon''(\omega)}{\varepsilon'(\omega)}. \quad (10)$$

We started dielectric studies of the REO films by examining the fundamental material properties and characteristics for ytterbium oxide films fabricated with different methods [23], [34]–[36]. At room temperature M/Yb₂O₃/M thin film capacitors exhibit high dielectric breakdown field strength, $F_b > 10^8$ V/m, the dielectric permittivity in the range of 10.9–12.5 (at 1 kHz), low dissipation factor, $\tan \delta = 0.004$ – 0.015 and temperature coefficient of the capacitance, TCC = 370 ppm/K.

In order to examine the basic dielectric properties of R₂O₃ films and M/R₂O₃/M thin film structures the dielectric measurements were carried out in a wide frequency range from 0.01 mHz to 10 MHz. A few experimental techniques, schematically shown in Fig.11 were applied for this aim [34], [37], [39]–[41], [43], [45], [52]. Experimental results were presented in the frequency domain with the following functions: $C'(f)$ and $C''(f)$ [41], [44], [45], $C'(f)$ and $\tan \delta$ [37], [39], [40], $\varepsilon'(f)$ and $\varepsilon''(f)$ [47], [48], [54], [58] or with dielectric susceptibility [42].

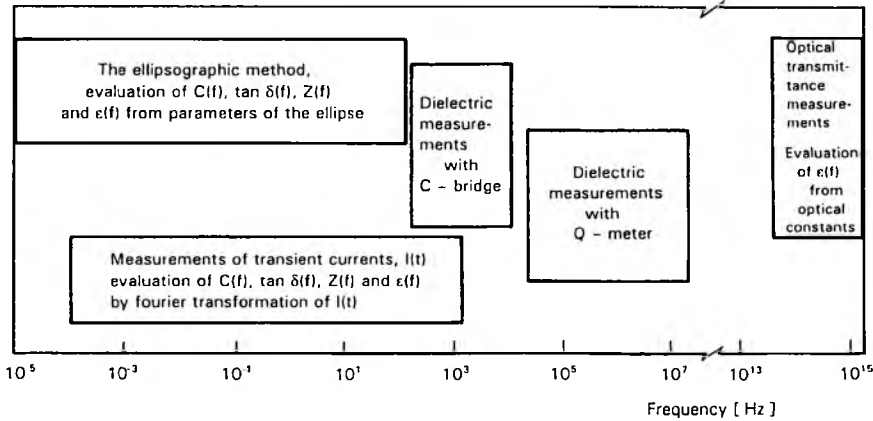


Fig. 11. Schematic illustration of experimental methods applied to dielectric measurements of rare earth oxide films in a wide frequency range.

6.1. Complex capacitance

Dispersion characteristics of the complex capacitance for $M/R_2O_3/M$ thin film capacitors ($R \equiv Dy, Ho$ and Yb) were very similar. Typical examples of C' and C'' dispersion curves obtained for $Al/Dy_2O_3/Al$ thin film sandwiches [41] measured at different temperatures are shown in Figs. 12 and 13. For low temperatures and high

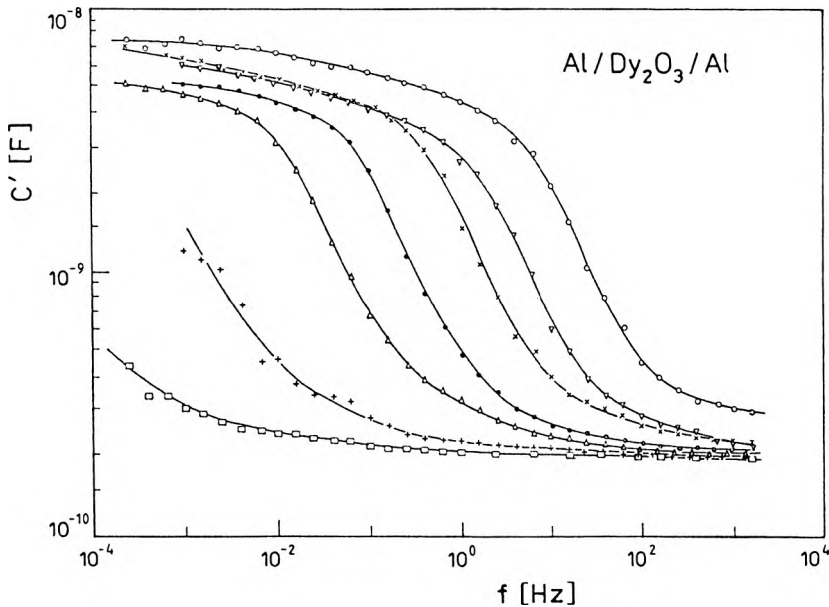


Fig. 12. Frequency dependence of the real part of the complex capacitance $C^*(f)$ at different temperatures: \circ - 476 K, ∇ - 451 K, \times - 428 K, \bullet - 398 K, Δ - 376 K, $+$ - 338 K, and \square - 298 K. Film thickness $d = 526$ K.

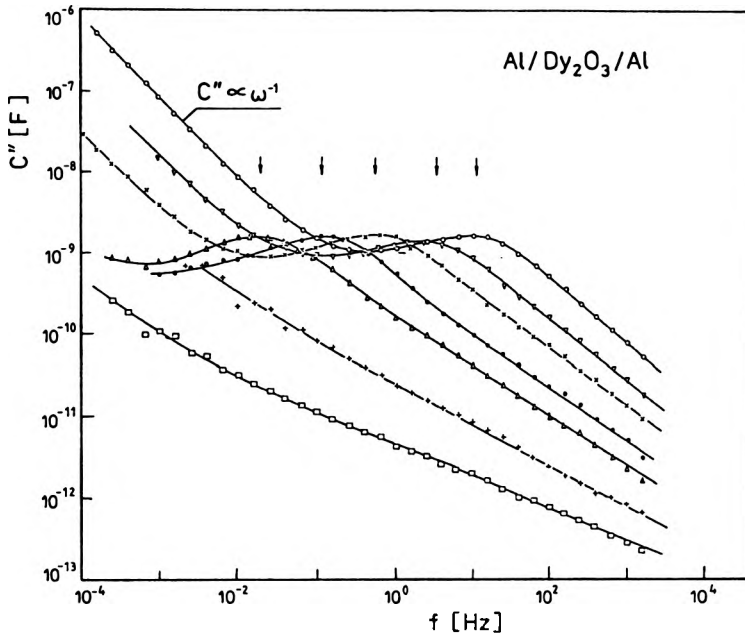


Fig. 13. Frequency dependence of the imaginary part of the complex capacitance $C''(f)$, for Al/Dy₂O₃/Al thin film sandwiches measured at different temperatures: \circ – 476 K, ∇ – 451 K, \times – 428 K, \bullet – 398 K, Δ – 376 K, $+$ – 338 K, and \square – 298 K. Film thickness $d = 526$ nm. Curves of the dielectric losses $C''(f)$ were evaluated from the charging currents. $C'' \propto \omega^{-1}$ is drawn to indicate the region dominated by d.c. conduction.

frequencies $C'(f)$ characteristics exhibit a small dispersion giving dielectric response of Dy₂O₃ film itself. At low frequencies $C'(f)$ curves increase strongly and saturate. The dissipation curves C'' for Al/Dy₂O₃/Al structures exhibit thermally activated peak, which comes from an interaction between the volume and interfacial processes [55]. The activation energy for the loss peak was estimated with Debye's shift method. Values of E_p were: 1–1.1 eV for Dy₂O₃ [40], [41] and Yb₂O₃ [40], [43] and 0.7 eV for Ho₂O₃ [58], respectively.

6.2. Dielectric permittivity

Figure 14 shows typical examples of dielectric response for dysprosium, holmium and ytterbium oxides sandwiched between aluminium electrodes [54]. Well-exposed, thermally activated maximum of dielectric losses is well seen in each curve. The real part of dielectric permittivity exhibits dispersion from one to three decades for frequency range between very low frequencies (*i.e.*, 10 μ Hz–100 μ Hz) up to radio frequencies. For low frequencies and high temperatures ϵ' saturated or even further increase of $\epsilon'(f)$ was observed [39], [40]. The dielectric permittivity in this range reached values from $\epsilon' = 100$ to $\epsilon' = 10000$. Such high values of dielectric permittivity evaluated in this range have been taken as the apparent dielectric permittivity for M/R₂O₃/M structures and they cannot be connected with material properties of

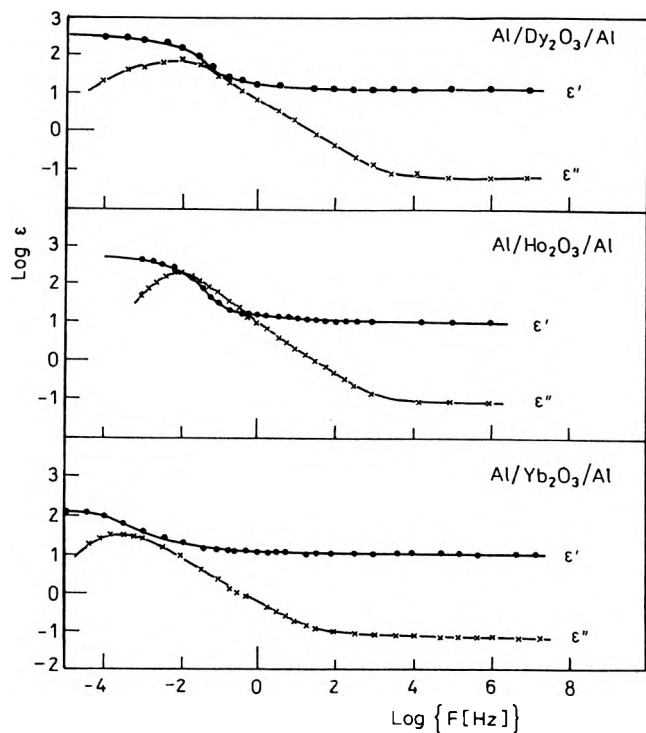


Fig. 14. Frequency dependence of the real and imaginary parts of dielectric permittivity for Al/R₂O₃/Al thin film structures. The results were obtained at a temperature of 376 K for Dy₂O₃, 425 K for Ho₂O₃ and at 355 K for Dy₂O₃. The experimental data correspond with insulator thickness of 526 nm, 216 nm and 150 nm for Dy₂O₃, Ho₂O₃ and Yb₂O₃, respectively.

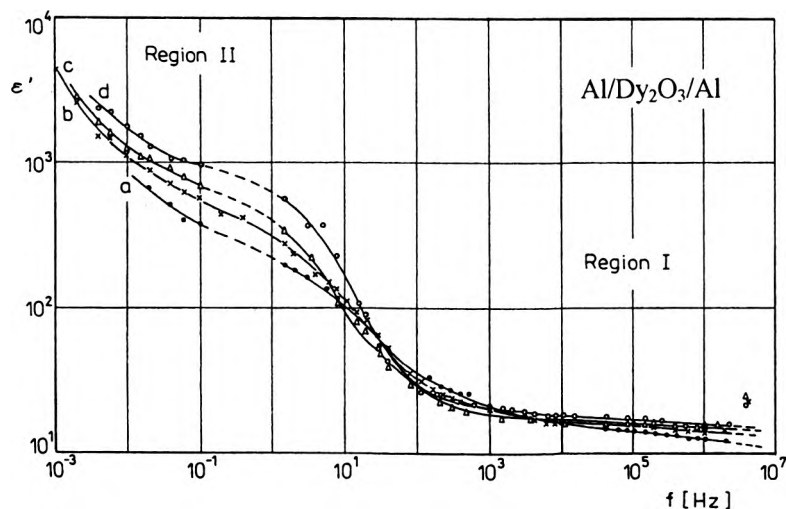


Fig. 15. Frequency dependence of ϵ' for Al/Dy₂O₃/Al thin film sandwiches of different dielectric thicknesses: a — 167 nm, b — 226 nm, c — 273 nm, d — 348 nm at a temperature of 543 K.

the oxides examined. This conclusion has been drawn on the basis of different experimental tests, *i.e.*, from examination of the influence of: i) the insulator thickness, ii) the voltage bias, iii) the temperature and iv) the material applied as electrodes, on dielectric properties of $M/R_2O_3/M$ structures [39], [40], [44], [54], [58]. In Figure 15 the influence of the film thickness on $\epsilon'(f)$ dispersion curves for $Al/Dy_2O_3/Al$ structures is shown. Two regions corresponding with properties of Dy_2O_3 volume (region I) and with properties of Al/Dy_2O_3 boundaries (region II) can be distinguished in this Figure. In region I, *i.e.*, for audio and radio frequency region a dispersion of ϵ' is very small. For different specimens values of the high frequency permittivity were in the range from 10 to 16. Values of the high-frequency permittivity depended on conditions during preparation of insulating films (mainly on the temperature of substrates, rate of film deposition and on oxygen pressure during evaporation process). We observed that the permittivity depended on the insulator thickness. A dependence of ϵ' on insulator thickness for ytterbium-oxide-based thin film capacitors is shown in Fig. 16. It can be seen that the permittivity is constant only for insulator thickness greater than about 80 nm ($\epsilon' = 12.5$). For thinner films ϵ' decreases down to about 7 [34]. In the same figure results obtained for the other rare earth oxides are compiled. Except of the anomalous behaviour observed by SAXENA and SRIVASTAVA [86] for Er_2O_3 results for different oxides are very similar. Such a dependence of dielectric permittivity on film thickness can be explained particularly by the porosity of very thin films and mainly by the influence of both near electrode regions (their contribution for a small insulator thickness can be important) [34], [36], [58].

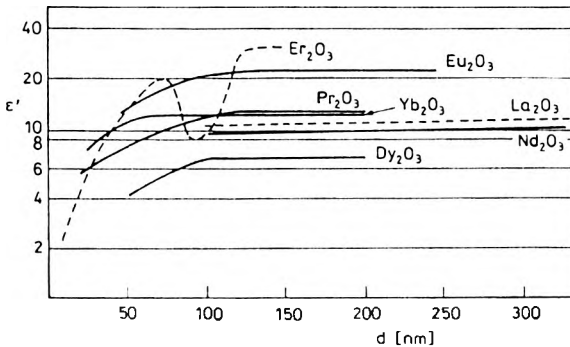


Fig. 16. Dependence of dielectric permittivity for $Al/Yb_2O_3/Al$ thin film capacitors. Results for Er_2O_3 [84], Eu_2O_3 [90], Pr_2O_3 [77], Dy_2O_3 [79] and La_2O_3 [96] are taken from the literature.

Finally, for optical frequencies the permittivity was evaluated from Maxwell relations and optical transmittance measurements [61]–[62]. Values of the high-frequency optical dielectric permittivity of R_2O_3 films were in the range from $\epsilon'_{\infty} = 3.24$ to $\epsilon'_{\infty} = 4.04$ and are given in Table 2.

To sum up the results presented in this chapter, the fundamental dielectric properties of the REO films have been compiled in Table 2. The literature data

dealing with the REO films prepared by electron-beam deposition have also been included in the same Table. It is seen that at room temperature the REO films exhibit interesting dielectric properties: i) relatively low dielectric losses, ii) low

Table 2. Fundamental dielectric properties of electron-beam deposited REO thin films at a temperature of 297 K: the dielectric permittivity ϵ' , the loss factor $\tan \delta$ and temperature coefficient of the capacitance TCC at 1 kHz, the dielectric permittivity ϵ'_{∞} at optical frequencies and the dielectric breakdown field strength F_b .

Rare earth oxide	ϵ'	$\tan \delta$	F_b [MV/cm]	TCC [ppm/K]	ϵ'_{∞}	References
La ₂ O ₃	12.2	0.004	0.2–2.2			[96]
CeO ₂	13	0.015				[97]
Pr ₂ O ₃					4.04	[28]
Nd ₂ O ₃	10.1					[96]
	12.64	0.0045	> 1.5	350		[94]
Eu ₂ O ₃	22.4	0.015		1200	3.39	[24], [90]
	11	0.015	2			[97]
Gd ₂ O ₃					3.65	[30]
	10		> 3			[116]
Tb ₂ O ₃					3.35	[27]
Dy ₂ O ₃	10.2–10.9	0.001			3.42	[41], [48]
	13.5			230–300		[40], [44]
Ho ₂ O ₃	10.8	0.01		150–210	3.24	[63]
	13–14	0.0075	3			[97]
Er ₂ O ₃					3.5	[26]
	13–14	0.007	4			[97]
Yb ₂ O ₃	10.9				3.62	[36], [54]
	12.5	0.004–0.015	> 1	370		[34], [40]
Lu ₂ O ₃					3.46	[62]
Y ₂ O ₃	13	0.003	3			[89]

TCC, iii) high dielectric breakdown field strength. Values of the dielectric permittivity (at 1kHz) for most of these oxides are in the range 10–14 and are close to values of ϵ' obtained from the dielectric measurements of bulk specimens ($11.5 < \epsilon' < 15.5$, except of CeO₂) or estimated from Lyddane–Sachs–Teller relation ($11.6 < \epsilon' < 14.9$) [117].

7. Complex impedance diagnostics

The dielectric data for MIM structures can be described also with their complex impedance or admittance [56]:

$$Z^*(\omega) = Z'(\omega) - jZ''(\omega) = R_s - \frac{j}{\omega C_s}, \quad (11)$$

$$Y^*(\omega) = Y'(\omega) + jY''(\omega) = G_p + j\omega C_p. \quad (12)$$

The complex impedance of MIM structure is connected with series resistance R_s and series capacitance C_s of a specimen. The complex admittance of a specimen is connected with its parallel resistance R_p ($R_p = G_p^{-1}$) and parallel capacitance C_p . Both of these quantities are connected by the relation

$$Z^*(\omega) = \frac{1}{Y(\omega)}. \quad (13)$$

Experimental data of any specimen can be presented with quantities Z or Y in the frequency domain as well as in the complex impedance or admittance graphs. The complex impedance diagnostics has been applied by us for examinations of the Al/ R_2O_3 /Al thin film structures ($R \equiv Dy, Ho$) in the frequency range $10^{-4} - 10^7$ Hz [46], [52], [55], [56], [58]. Figures 17 and 18 show examples of the complex

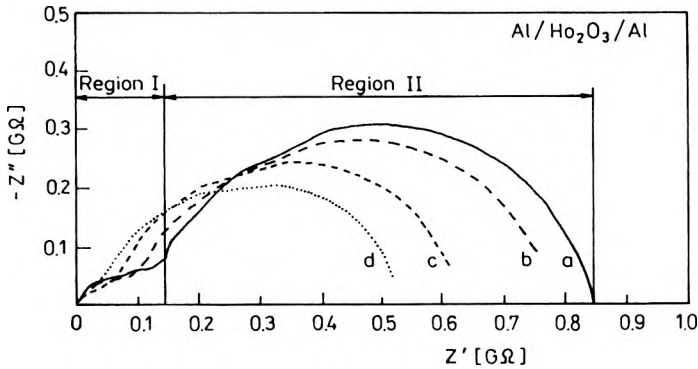


Fig. 17. Complex impedance graphs for Al/ Ho_2O_3 /Al thin film capacitors. Results obtained for different insulator film thicknesses: a – 273 nm, b – 216 nm, c – 130 nm and d – 52 nm.

impedance graphs (the imaginary Z versus real Z) obtained for Al/ Dy_2O_3 /Al and Al/ Ho_2O_3 /Al thin film structures of a different film thicknesses (Fig. 17) [52], [58] and for different voltage bias (Fig. 18) [56]. Two separate regions have been distinguished in each $Z'' = F(Z')$ graph:

- i) the high frequency region corresponding to the volume of the insulating film (region I), and
- ii) the low-frequency region connected with properties of M/I interfaces (region II).

A detailed analysis carried out for Dy_2O_3 and Ho_2O_3 -based thin film capacitors enabled estimation of a resistance of the volume of the insulator and a resistance of M/I interfaces [52], [56]. Both of these resistances were thermally activated. The activation energy for the volume processes was 1 eV and 0.7 eV for Dy_2O_3 and Ho_2O_3 , respectively and corresponded with the activation energies of the dielectric loss peak. The resistivity of M/I boundaries was extremely high and a complete semicircle or arc was rarely observed even for high temperatures and frequencies as low as 0.1 mHz. Very often only a "spur" very sensible to the measurement voltage

was formed in this region. The activation energy estimated in this region for Al/Dy₂O₃/Al structures $E_b = 1.2$ eV was slightly higher than for the volume processes [56].

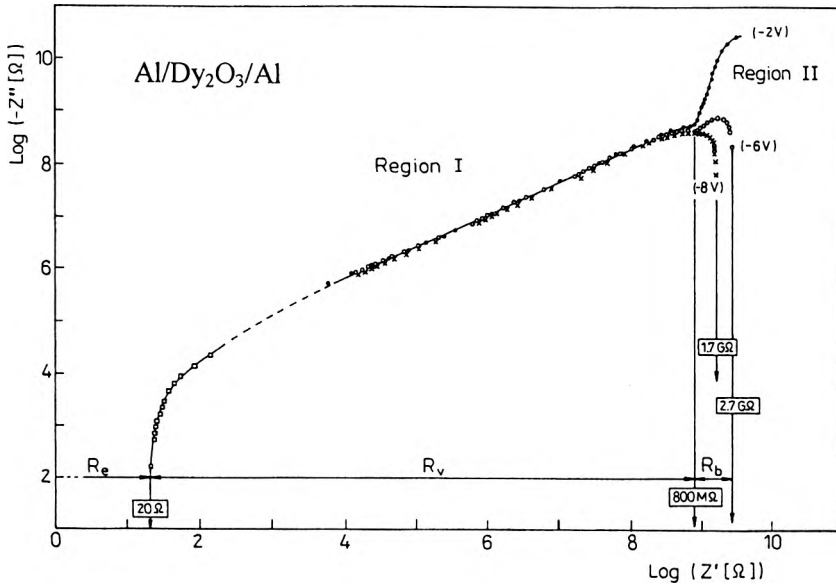


Fig. 18. Influence of the measurement voltage ($U = -2, -6$ and -8 V) on the complex impedance graphs for Al/Dy₂O₃/Al thin film capacitors at the temperature $T = 411$ K. Resistance of electrodes R_e , the insulator R_v and barriers R_b are indicated.

We should also mention that dielectric studies at "high voltages" enable observation of a transition from electrode limited processes to volume limited processes. In general, high electric voltages cause large deformation of region II in $Z'' = F(Z')$ graphs. Unfortunately, very often it corresponds with irreversible changes in MIM structures, which usually are much faster at high temperatures [56]. The complex impedance graphs enable also estimation of the resistance of capacitor electrodes and contacts of M/R₂O₃/M structures [56].

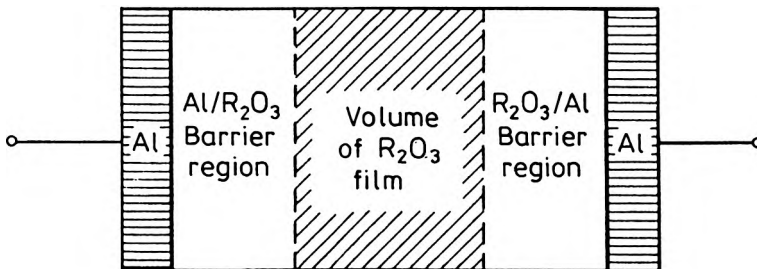


Fig. 19. Schematic illustration of M/R₂O₃/M thin film structure showing the volume region of R₂O₃ film and two interfacial M/R₂O₃ regions at each metal/insulator boundary.

These examinations lead us to conclusion that $M/R_2O_3/M$ thin film structures can be represented by a simple model schematically shown in Fig. 19 [54], [56]. In this model, three regions, namely: the region of the volume of R_2O_3 film and two near-electrode regions (Schottky barrier regions) are connected with metal electrodes. It has been shown that 4–8 nm thick Schottky barriers are formed at each electrode [39], [54].

8. Thermally stimulated processes (TSDC, TSPC and TSEE)

Different thermally stimulated techniques such as the thermoluminescence (TL), thermally stimulated electron emission (TSEE), thermally stimulated capacitance (TSCAP), thermally stimulated currents (TSC), *i.e.*, thermally stimulated depolarization currents (TSDC), and thermally stimulated polarization currents (TSPC) have been widely applied for electrical studies of semiconductors or insulators sandwiched between metallic electrodes.

The TSC and the TSEE methods have been applied by us for examination of R_2O_3 thin films ($R = Dy, Ho$ and Yb).

8.1. Thermally stimulated currents

The TSC measurements were carried out in the temperature range from 130 K (297K) to about 550 K. The TSDC thermograms were obtained by specimens heating at a constant rate β , so that the temperature increased linearly with time: $T = T_0 + \beta t$. Microcomputer controlled apparatus for recording the TSC spectra have been described in the papers [49]–[51].

The low-temperature measurements carried out for $Al/Yb_2O_3/Al$ thin film thermoelectrets show that TSDC spectra exhibit only a single peak at 299 K connected with the trapping level of 0.25 eV [38]. Systematic examinations of the TSDC and TSPC spectra were performed for the temperature range 297 K–500(550) K [47], [49]–[51], [53]. The influence of the heating rate, the polarizing temperature and time, the polarization voltage as well as the sample thickness on the TSDC and TSPC characteristics was tested. The TSDC spectra for $M/R_2O_3/M$ thin film structures were very similar. The TSDC thermograms for $Al/Ho_2O_3/Al$ thin film thermoelectrets measured at different heating rates β are shown in Fig. 20 [51]. The TSDC characteristics are characterized by a single peak located between 360 K and 400 K depending on the rate of heating. It was established, however, that for high temperatures (*i.e.*, for $T > T_m$, where T_m is the temperature for the TSDC peak) a shape of TSDC characteristics is complex and depends on the polarization voltage, on the polarization time and polarization temperature [50], [51]. For the positive polarization voltage applied to the upper electrode the TSDC increases monotonically with the temperature, whereas for the negative voltage reverses its sign. This difference in the high temperature TSDC characteristic could be related to an asymmetrical structure of each M/I boundary [51].

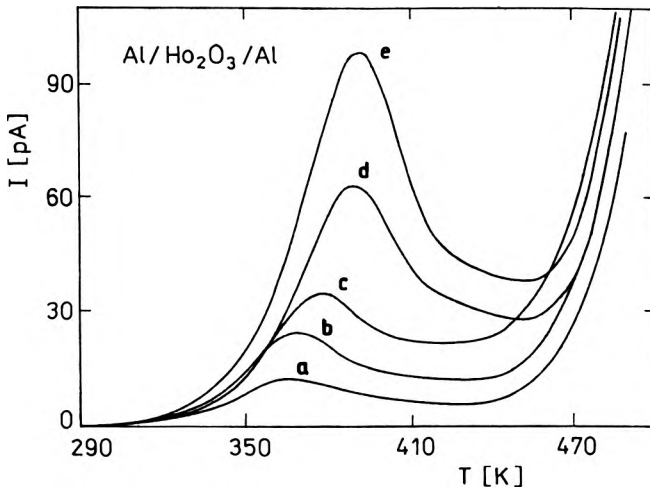


Fig. 20. TSDC curves for Al/Ho₂O₃/Al thin film capacitors measured at different heating rates: **a** – 0.042 K/s, **b** – 0.071 K/s, **c** – 0.12 K/s, **d** – 0.21 K/s, **e** – 0.3 K/s. Polarization conditions: $U_p = -1$ V, $t_p = 1000$ s, $T_p = 410$ K. Thickness of the insulator $d = 130$ nm.

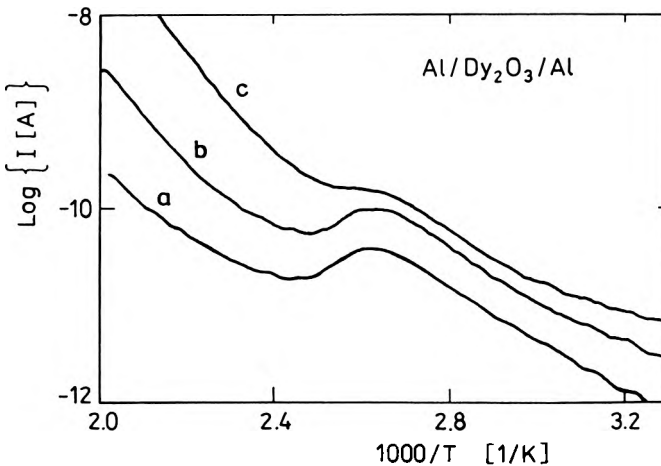


Fig. 21. TSPC curves for Al/Dy₂O₃/Al capacitors measured at different voltages: **a** – $U = 1$ V, **b** – $U = 2$ V and **c** – $U = 3$ V ($\beta = 0.21$ K/s, $d = 526$ nm).

The TSPC spectrum was measured after TSDC cycle at linear heating condition, *i.e.*, for $T = T_0 + \beta t$. The TSPC is a sum of the equilibrium current (responsible for d.c. conductivity) and the nonequilibrium current. Typical TSPC characteristics for Al/Dy₂O₃/Al thin film capacitors are shown in Fig. 21 [59]. The TSPC curves obtained for low voltages (for $U < 2.5$ V) exhibit a single maximum which strictly corresponds with the observed TSDC peak. For $U > 2.5$ V the TSPC peak disappears due to a large contribution of the conductivity current.

8.2. TSEE spectra

Examinations of the TSEE spectra were performed for Yb_2O_3 thin films deposited onto tungsten substrates [38]. The measurements of the exoelectrons were carried out in the temperature range 273–800 K. The TSEE characteristics exhibited well marked maximum at the temperature of about 770 K.

8.3. Activation energy of traps

Different methods have been proposed in the literature for determination of traps activation energy from thermally stimulated thermograms. We have estimated the traps activation energy with the method of GARLICK-GIBBSON [38]. This method takes into account the low temperature tail of the TSDC, TSPC and TSEE curves, where the measured signal follows according to the relation: $I(T) = I_0 \exp[-E/kT]$, in which I_0 is a constant and E is the activation energy of the process. The experimental data for R_2O_3 films and for $\text{M}/\text{R}_2\text{O}_3/\text{M}$ structures were presented in $\log I \sim 1000/T$ scale. The low temperature experimental results can be approximated by straight lines the slopes of which correspond to E . Values of the activation energies estimated for Yb_2O_3 films and for $\text{Al}/\text{Ho}_2\text{O}_3/\text{Al}$, $\text{Al}/\text{Dy}_2\text{O}_3/\text{Al}$ and $\text{Al}/\text{Yb}_2\text{O}_3/\text{Al}$ thin film structures are given in Tab. 3. In the same table values of the activation energies obtained in electrical conductivity measurements E_σ as well as by Debye's shift method in dielectric measurements E_p are compiled.

Table 3. The activation energies for R_2O_3 thin films estimated in thermally stimulated processes E_{TSD} , E_{TSP} , E_{TSEE} , from the dielectric measurements E_p and from electrical conductivity measurements E_σ .

Rare oxide oxide	E_{TSD} [eV]	E_{TSP} [eV]	E_{TSEE} [eV]	E_p [eV]	E_σ [eV]	References
Dy_2O_3	0.7					[49]
	0.6–0.8	0.55				[47]
				1–1.1	0.01–0.03	[39]–[41]
					1–1.2	[47]
Ho_2O_3					1.23	[58]
	0.5, 0.7	0.6–0.74			1	[50], [51]
Yb_2O_3				0.7		[55]
	0.25		1.6			[38]
	0.6–0.8					[59]
				1–1.1		[40], [43]
					0.53, 0.98	[36]

9. Photoconductivity

The photoconductivity of $\text{M}/\text{Gd}_2\text{O}_3/\text{Al}$ thin film structures with different metal electrodes ($\text{M} \equiv \text{Al}, \text{Cu}, \text{Cr}, \text{Ag}$ and Au) has been investigated by NOWAK [19], [20]. Photoconductivity current was measured at a temperature of 77 K and 300 K for

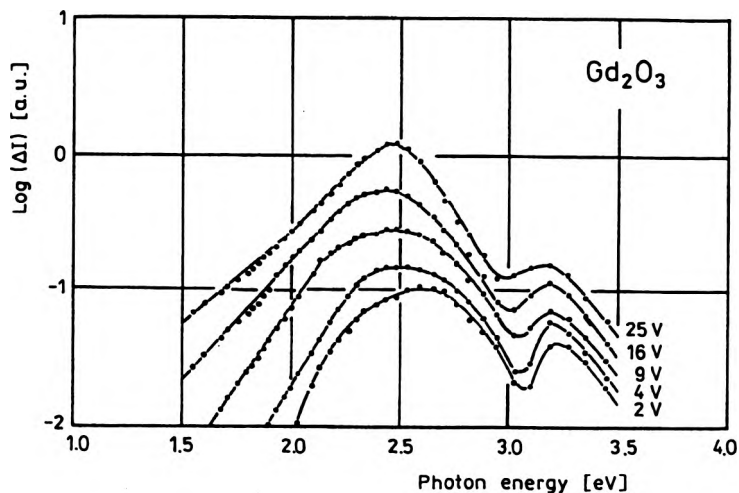


Fig. 22. Spectral characteristic of photocurrent at 300 K for an Al/Gd₂O₃/Al structure at a constant incident photon flux. The Gd₂O₃ film thickness was 230 nm and the top electrode was positive

specimens illuminated through semitransparent metal top electrodes with monochromatic radiation in the energy range $h\nu = 1.5 - 3.5$ eV. Under illumination the photocurrent shows a very weak temperature dependence between 77 K and 300 K. A typical spectral scan shown in Fig. 22 exhibits two peaks. The experimental data were interpreted as the bulk excited photoeffect [20].

10. Summary and conclusions

Results of our experimental investigations dealing with thin films of rare earth oxides have been presented. These studies may be summarized in the following way:

1. Rare earth oxide films were fabricated with different methods. We have shown that satisfactory (amorphous or polycrystalline) thin-film coatings can be fabricated with all the methods applied, except for evaporation of the REO from resistance heaters.

2. Rare earth oxide films prepared on quartz or glass were stable in time and exhibited very good adhesion.

3. Rare earth oxide thin-film coatings exhibit interesting optical properties. Films of sesquioxides are transparent over a wide spectral range and have the refractive index in the range 1.8–1.92 (at $\lambda = 0.55$ μm).

4. Electrical and dielectric studies were carried out for M/R₂O₃/M thin film structures ($R \equiv \text{Dy, Ho and Yb}$). Values of the estimated dielectric permittivity for thick films increase from $\epsilon'_{\infty} = 3.24 - 3.62$ at optical frequencies to $\epsilon' = 10 - 14$ for the audio- and radio-frequencies; and $\epsilon' = 100 - 10000$ (the apparent dielectric permittivity) at very low frequencies. In a wide frequency spectrum different polarization mechanisms are responsible for dielectric properties of R₂O₃ thin films and M/R₂O₃/M thin film structures.

5. The results presented lead us to conclusions that both volume of the oxide film and metal/insulator boundaries are important in electrical and dielectric examinations of $M/R_2O_3/M$ structures. Thin barriers, a few nanometers thick formed at both metal electrodes are responsible for low frequency/high temperature dielectric properties of these structures. High frequency/low temperature dielectric properties of $M/R_2O_3/M$ structures are connected with R_2O_3 film.

6. Thermally stimulated methods, the TSDC, TSPC and TSEE, as well as measurements of the photoconductivity were applied for examinations of traps in R_2O_3 thin films.

7. Optical characteristics show that rare earth oxide thin films can be considered as useful materials for fabrication of different good-quality thin-film optical coatings (especially as interference coatings). Moreover, very good dielectric and insulating properties classify them for application in electronic microcircuits.

References

- [1] EYRING L., *The Handbook on the Physics and Chemistry of Rare Earths*, [Ed.] K. A. Gschneider, L. Eyring, Vol. 3, North-Holland, Amsterdam 1979, pp. 337–399.
- [2] EYRING L., *Nonstoichiometric Oxides*, [Ed.] O. Toft Sorensen, Acad. Press., NY 1981, pp. 337–398.
- [3] EYRING L., *High Temperature Oxides*, Part II, [Ed.] Allen M. Alper, Acad. Press NY 1970, pp. 41–97.
- [4] GASNIER M., *Phys. Status Solidi A* **57** (1980), 11.
- [5] *Ibidem*, **114** (1989), 11.
- [6] ADASCHI G., IMANAGA N., *Chemical Rev.* **98** (1998), 1479.
- [7] SAMSONOV G.V., *Fiziko-Khimicheskie Svojstva Okislov. Spravochnik, Metalurgiya*, (in Russian) Moskva 1978, pp. 12–270.
- [8] ZHUZE W.P., SZELYKH A. I., *Phys. Techn. Semicond.* **23** (1989), 393.
- [9] BERRY R.W., HALL P.M., HARRIS M.T., *Thin Film Technology*, D. Van Nostrand Co., 1968.
- [10] GLANG R., *Handbook of Thin Film Technology*. [Ed.] L.I. Maissel, R. Glang, McGraw-Hill Book Co., NY 1970, pp. 1.3–1.130.
- [11] CHOPRA K.L., *Thin Film Phenomena*, McGraw-Hill Book Co., NY 1969.
- [12] CAMPBELL D.S., *Active and Passive Thin Film Devices*, [Ed.] T.J. Coutts, Acad. Press, London 1978, pp. 23–56.
- [13] BACH H., KRAUSE D., *Thin Films on Glass*, Chapters 1 and 3, Springer-Verlag, Berlin 1997.
- [14] HASS G., RAMSEY J.B., THUN R., *J. Opt. Soc. Am.* **49** (1959), 116.
- [15] PHILIPS W.L., *J. Less Common Metals* **7** (1964), 139.
- [16] FELDMAN C., HACKAYLO M., *Rev. Sci. Instrum.* **33** (1962), 1459.
- [17] RAIDEN J.C., *J. Electrochem. Soc.* **114** (1967), 75.
- [18] HALIMON M.M., RUDNIEV V.V., *Elektronnaya Tekhnika*, Ser. 14, vyp. 2 (1968), 103.
- [19] NOWAK G.B., *Physics of Thin Films*, [Ed.] by L. Żdanowicz, PWN, Warszawa 1981, pp. 508–511.
- [20] NOWAK G.B., *Thin Solid Films* **78** (1981), 187.
- [21] IDCZAK E., ŻUKOWSKA K., *Opt. Appl.* **8** (1978), 55.
- [22] ŻUKOWSKA K., IDCZAK E., *Thin Solid Films* **85** (1981), 327.
- [23] MARCINÓW T., WESOŁOWSKA C., WIKTORCZYK T., *Sci. Papers of the Institute of Electron Technology, Wrocław University of Technology*, (in Polish), No. 17 (1978), 91.
- [24] MARCINÓW T., [In] *Physics of Thin Films* [Ed.] L. Żdanowicz, PWN, Warszawa 1981, pp. 483–485.
- [25] MARCINÓW T., WESOŁOWSKA C., WIKTORCZYK T., *Opt. Appl.* **7** (1977), 135.
- [26] MARCINÓW T., TRUSZKOWSKA K., *Appl. Opt.* **20** (1981), 1755.

- [27] MARCINÓW T., WESOŁOWSKA C., ŻUKOWSKA K., *Opt. Appl.* **15** (1985), 249.
- [28] MARCINÓW T., *Opt. Appl.* **17** (1987), 131.
- [29] TRUSZKOWSKA K., MARCINÓW T., WESOŁOWSKA C., *Opt. Appl.* **4** (1974), 17.
- [30] TRUSZKOWSKA K., WESOŁOWSKA C., *Opt. Appl.* **7** (1977), 55.
- [31] TRUSZKOWSKA K., WESOŁOWSKA C., *Thin Solid Films* **31** (1976), 391.
- [32] TRUSZKOWSKA K., BOROWICZ T., WESOŁOWSKA C., *Appl. Opt.* **17** (1978), 1579.
- [33] TRUSZKOWSKA K., *Opt. Appl.* **10** (1980), 139.
- [34] WIKTORCZYK T., WESOŁOWSKA C., *Thin Solid Films* **71** (1980), 15.
- [35] WIKTORCZYK T., [In] *Physics of Thin Films*, Ed. L. Żdanowicz, PWN, Warszawa 1981, pp. 454–458.
- [36] WIKTORCZYK T., WESOŁOWSKA C., *Thin Solid Films* **91** (1982), 9.
- [37] WIKTORCZYK T., WESOŁOWSKA C., *Thin Solid Films* **120** (1984), 171.
- [38] WIKTORCZYK T., WESOŁOWSKA C., *Physica Status Solidi A* **82** (1984), K67.
- [39] WIKTORCZYK T., Proc. 2nd Int. Conf. on *Conduction and Breakdown in Solid Dielectrics*, July 7–10, 1986, Erlangen, Germany, IEEE/EIS, Cat. No. 86CH2124-6, 1986, pp. 222–226.
- [40] WIKTORCZYK T., WESOŁOWSKA C., *Vacuum* **37** (1987), 107.
- [41] WIKTORCZYK T., NITSCH K., BOBER Z., *Thin Solid Films* **157** (1988), 13.
- [42] WIKTORCZYK T., *Solid State Commun.* **67** (1988), 143.
- [43] WIKTORCZYK T., *Material Sci.* **14** (1988), 31.
- [44] WIKTORCZYK T., Proc. 6th Int. Symp. on Electrets, Oxford, September 1–3, 1988, England, IEEE/EIS Cat. No. 88CH2593-2, 1988, pp. 607–611.
- [45] WIKTORCZYK T., NITSCH K., BOBER Z., Proc. 3rd Int. Conf. on *Conduction and Breakdown in Solid Dielectrics*, July 3–6, 1989, Trondheim, Norway, IEEE/EIS, Cat. No. 89CH 2726-8, 1989, pp. 202–206.
- [46] WIKTORCZYK T., Proc. 1st Symposium on *Low Frequency Dielectric Spectroscopy and Related Problems*, September 15–20, 1990, Krynica (Poland), pp. 71–77.
- [47] WIKTORCZYK T., *Material Sci.* **16** (1990), 243.
- [48] WIKTORCZYK T., *Eur. J. Solid State Inorg. Chem.* **28** (1991), 581.
- [49] WIKTORCZYK T., Proc. 13th Conf. ISHM, October, 9–12, 1989 Szklarska Poręba, Poland, [Ed.] Int. Soc. Hybrid Microel., Poland Chapter, Wrocław 1990, pp. 76–78.
- [50] WIKTORCZYK T., Proc. 7th Int. Symp. Electrets, September 25–27, 1991, Germany, IEEE/EIS Cat. No. 91CH3029, 1991, pp. 675–680.
- [51] WIKTORCZYK T., *IEEE Trans. Electrical Insulation* **27** (1992), 807.
- [52] WIKTORCZYK T., NITSCH K., BOBER Z., Proc. 4th Int. Conf. *Conduction and Breakdown in Solid Dielectrics*, June 22–25, 1992, Sestri Levante, Italy, IEEE/EIS, Cat. No. 92CH3034-6, 1992, 87–91.
- [53] WIKTORCZYK T., Proc. 3rd Int. Conf. *Dielectric and Related Phenomena*, September 12–16, 1994, Zakopane (Poland), [Ed.] Techn. Univ. of Łódź Branch Bielsko-Biała, (Poland), 1997, pp. 137–143.
- [54] WIKTORCZYK T., [In] *Equilibrium Structure and Properties of Surfaces and Interfaces*, [Ed.] A. Gonis and G.M. Stocks, Plenum Press, New York 1992, 341–346.
- [55] WIKTORCZYK T., *Folia Scientiarum Universitatis Technicae Resoviensis, Matematyka i Fizyka* **102** 1992, 23–25.
- [56] WIKTORCZYK T., *Physica Status Solidi A* **139** (1993), 397.
- [57] WIKTORCZYK T., Proc. 8th Int. Symp. on Electrets, September 7–9, 1994, Paris, IEEE/EIS, 1994, pp.325–330.
- [58] WIKTORCZYK T., Proc. 5th Int. Conf. *Conduction and Breakdown in Solid Dielectrics*, July 10–13, 1995, Leicester, England, IEEE/EIS, Cat. No. 95CH3476-9, 1995, pp. 64-68.
- [59] WIKTORCZYK T., Proc. SPIE **3181** (1997), 85.
- [60] WIKTORCZYK T., Proc. SPIE **37DP** (1998), 121.
- [61] WIKTORCZYK T., Report of the Institute of Physics, Technical University of Wrocław, No. 53, 1998.
- [62] WIKTORCZYK T., POPRAWKA J., Proc. 10th Int. Symp. on Electrets, September 22–24, 1999, Delphi, Greece, IEEE/EIS, Cat. No. 99CH36256, 1999, pp. 705–708.
- [63] WIKTORCZYK T., *Ibidem*, pp. 135–138.

- [64] TRUSZKOWSKA, *Optical properties of gadolinium oxide films*, Ph.D. Thesis (in Polish), Wrocław University of Technology, 1977.
- [65] Marcinow T., *Physical properties of ytterbium oxide films*, Ph.D. Thesis (in Polish), Wrocław University of Technology, 1975.
- [66] WIKTORCZYK T., *Electrical properties of ytterbium oxide films*, Ph.D. Thesis (in Polish), Wrocław University of Technology, 1982.
- [67] STEWARD M., *Brit. J. Appl. Phys.* **2** (1962), 159.
- [68] TAKAGI K., FUKAZAWA T., SUSA K., *J. Appl. Phys.* **61**, (1987), 1030.
- [69] GOSWAMI A., GOSWAMI A.P., *Thin Solid Films* **27** (1975), 123.
- [70] FROMHOLD A.T., *Physica Status Solidi* **36** (1969), 129.
- [71] YAYARAJ M.K., VALLABHAN C.P.G., *Thin Solid Films* **177** (1989), 59.
- [72] YAYARAJ M.K., VALLABHAN C.P.G., *Bull. Electrochem.* **5** (1989), 284.
- [73] CHANDRA SHEKAR M., HARI BUBU V., *Cryst. Res. Technol.* **19** (1984), 1405.
- [74] *Ibidem*, p. 1649.
- [75] *Ibidem*, p. 721.
- [76] *Ibidem*, p. 1521.
- [77] GOSWAMI A., GOSWAMI A.P., *Thin Solid Films* **20** (1974), S3.
- [78] *Ibidem*, **22** (1975), S2.
- [79] *Ibidem*, **28** (1975), 157.
- [80] DAKHEL A. A., *Physica Status Solidi A* **147** (1995), K79.
- [81] DUTTA C.R., BARUA K., *Thin Solid Films* **100** (1983), 149.
- [82] *Ibidem*, **92** (1982), 281.
- [83] *Ibidem*, **103** (1982), 295.
- [84] SAXENA U., SRIVASTAVA O.N., *Thin Solid Films* **33** (1976), 185.
- [85] *Ibidem*, **42** (1977), L1.
- [86] HEITMANN W., *Appl. Opt.* **12** (1973), 394.
- [87] FROMHOLD A.T., FOSTER W. D., *Electrocomp. Sci. Technol.* **3** (1976), 52.
- [88] SINGH A., *Thin Solid Films* **105** (1983), 163.
- [89] TSUTSUMI T., *Jpn. J. Appl. Phys.* **9** (1970), 735.
- [90] NAKANE H., NOYA A., KURIKI S., MATSUMOTO G., *Thin Solid Films* **59** (1979), 291.
- [91] MAHALINGHAM T., RADHAKRISHNAN M., BALASUBRAMANIAN C., *Thin Solid Films* **78** (1981), 229.
- [92] RIEMAN E., YOUNG L., *J. Appl. Phys.* **44** (1973), 1044.
- [93] ŻDANOWICZ T., *Thin Solid Films* **164** (1988), 175.
- [94] DHARMADHIKARI V.S., GOSWAMI A., *Thin Solid Films* **87** (1982), 119.
- [96] IRLIN A.V., VLASOVA V.V., FABRIKANT B.A., *Polupr. Tekh. Mikroel.*, vyp. 24 (1976), 80 (in Russian).
- [97] KRIKOROV V.S., KRASOV V.G., MARKARIANC A.E., *Elektron. Tekhnika*, ser. 12, vyp. 1 (1971), 79 (in Russian).
- [98] CERNOBROVKIN D.I., BAKHTINOV V.V., SAKHAROV YU., *Prib. Tekh. Eksp.* No. 3 (1971), 159 (in Russian).
- [99] OSIPOV K.A., KRASOV V.G., ORLOV I.I., KHROMOV A.D., *Izv. Acad. Nauk SSSR, Neorg. Mat.* **12** (1976), 125.
- [100] KUTTY T.R.N., *Thin Solid Films* **127** (1985), 223.
- [101] KALKUR T.S., KWOR R.Y., PAZ DE ARAUJO C.A., *Thin Solid Films* **170** (1989), 185.
- [102] NAKAZAWA T., INOUE T., SATOH M., YAMAMOTO Y., *Jpn. J. Appl. Phys.* **34** (1995), 548.
- [103] CAMPBELL C.K., THEWALT M., *Thin Solid Films* **13** (1972), 195.
- [104] SAYER M., MARTIN M.S., HELLICAR N.J., *Thin Solid Films* **6** (1976), R61.
- [105] HEAVENS O.S., *Physics of Thin Films*, [Eds.] Hass G., Thun R.E., Vol. 2 (1964), 193.
- [106] DOBIERZEWSKA-MOZRZYMAS E., LEWANDOWICZ S., MOZRZYMAS J., *Acta Phys. Pol. A* **41** (1972), 251.
- [107] HALL J.F., FERGUSSON W.F., *J. Opt. Soc. Am.* **45** (1954), 714.
- [108] SCHULTZ L.G., TANGERLINI F.K., *J. Opt. Soc. Am.* **44** (1954), 362.

- [109] VRIENS L., RIPPENS W., Appl. Opt. **22** (1983), 4105.
- [110] SUBBA RAO G. V., RAMDAS S., MEHROTRA P. N., RAO C. N. R., J. Sol. State Chem. **2** (1970), 377.
- [111] BOGORODITSKIY N. P., PASYNKOV V. V., BASILI R. R., VOLOKOBINSKIY YU. M., Dokl. Akad. Nauk SSSR **160** (1965), 578 (in Russian).
- [112] NEUJMIN A. D., BALAKIREVA V. B., NALGUEV S. F., Dokl. Akad. Nauk SSSR **209** (1973), 1150 (in Russian).
- [113] NODDACK W., WALCH H., Z. Electrochem. **63** (1959), 269.
- [114] WERON K., J. Phys. C, Condensed Matter **3** (1992), 9151.
- [115] JONSCHER A. K., Thin Solid Films **100** (1986), 329.
- [116] HONG W., KWO J., KORTAN A. R., *et al.*, Science **283** (1999), 1897.
- [117] DULEPOV E. V., BATSANOV S. S., KUSTOVA G. N., Zh. Strukt. Khimii **13** (1972), 935 (in Russian).

Received June 13, 2000